Published in final edited form as:

Nat Mater. 2015 November ; 14(11): 1104–1109. doi:10.1038/nmat4364.

Nanocapillarity-mediated magnetic assembly of nanoparticles into ultraflexible filaments and reconfigurable networks

Bhuvnesh Bharti[1], **Anne-Laure Fameau**[2], **Michael Rubinstein**[3], and **Orlin D. Velev**[1,★]

Orlin D. Velev: odvelev@ncsu.edu

[1]Department of Chemical and Biomolecular Engineering, North Carolina State University, Raleigh, North Carolina 27695-7905, USA

[2]National Institute of French Agricultural Research, Nantes 44300, France

[3]Department of Chemistry, University of North Carolina, Chapel Hill, North Carolina 27599-3290, USA

Abstract

The fabrication of multifunctional materials with tunable structure and properties requires programmed binding of their building blocks[1,2]. For example, particles organized in long-ranged structures by external fields[3,4] can be bound permanently into stiff chains through electrostatic or van der Waals attraction[4,5], or into flexible chains through soft molecular linkers such as surface-grafted DNA or polymers[6–11]. Here, we show that capillarity-mediated binding between magnetic nanoparticles coated with a liquid lipid shell can be used for the assembly of ultraflexible microfilaments and network structures. These filaments can be magnetically regenerated on mechanical damage, owing to the fluidity of the capillary bridges between nanoparticles and their reversible binding on contact. Nanocapillary forces offer opportunities for assembling dynamically reconfigurable multifunctional materials that could find applications as micromanipulators, microbots with ultrasoft joints, or magnetically self-repairing gels.

Mixtures of sand and water (as in sandcastles) are one of the best known examples of a reconfigurable material. The water wets the surface of the grains and forms capillary bridges between them, holding the sand particles together into a complex shape[12]. Similarly, capillary forces also offer unconventional ways to assemble particles on the microscale[13]. In many cases, attractive capillary forces can be stronger than conventional colloidal forces, such as van der Waals and repulsive electrostatic forces[14]. Even a small amount of liquid immiscible with the continuous phase and wetting the particles induces particle attraction via capillary bridges and completely changes the viscoelastic properties of the suspension[15]. Capillary forces provide strong reversible binding of the colloidal particles in liquid media at

★Correspondence and requests for materials should be addressed to O.D.V.

Additional information: Supplementary information is available in the online version of the paper.

Author contributions: B.B., A.-L.F. and O.D.V. conceived and designed the experiments. B.B. and A.-L.F. performed the experiments. M.R. proposed the persistence-length analysis and interpretation of filament flexibility. B.B. performed the experimental data analysis. B.B. and O.D.V. wrote the manuscript. All authors read and commented on it.

Competing financial interests: The authors declare no competing financial interests.

the microscale and mesoscale[16], and lead to complex surface architectures at the sub-micrometre length scale[17]. However, to our knowledge, the presence of capillary bridging forces at the nanoscale has not been reported or used as a tool for nanoparticle binding in liquid media. We report here how capillary forces could be used to form magnetically directed assembly of nanoparticles surrounded by a surface-condensed liquid lipid layer. In the presence of a magnetic field these nanoparticles form filaments and two-dimensional (2D) gels. Similar structures are of specific interest in the field of biomedicine, electronics, soft robotics and sensors[1,18]. The nature of the binding potential between the particles determines the stiffness, tensile strength and other physical properties of the structure. Permanently bound chains have been assembled previously by aligning them in an external magnetic field of particles adsorbed on the walls of surfactant microtubules[19] or colloidal particles with a thick grafted layer of a covalent linker[19–21]. These approaches require synthetic chemistry methods and lead to irreversible assembly.

The nanoscale units for our magnetic nanocapillary assembly experiments were obtained by dispersing spheroidal 20–30 nm γ-Fe_2O_3 maghemite nanoparticles into aqueous solutions of fatty acid salts. An external magnetic field was used to drive the particle assembly into chain-like filaments. The experimental set-up is schematically shown in Fig. 1a. The dynamics of the system was monitored by optical microscopy and was divided into two distinct steps, as illustrated in Fig. 1b. In the first step, the magnetic particles and their microaggregates were pulled together and organized in filament- and fibre-like assemblies along the direction of the applied field (Fig. 1c,d). In the subsequent step, switching off the magnetic field removes the field-induced attraction and relaxes the extended chains, but the filaments remained intact. The aligned fibre-like structures moved freely with the surrounding fluid flow and adapted highly undulating relaxed configurations (Fig. 1e and Supplementary Movie 1). The superconducting quantum interference device (SQUID) magnetization curves show some residual magnetic moment in the nanoparticles (Supplementary Fig. 2). This residual polarization can be attributed to the increase in size of the stable single-domain and to the presence of multidomains in the nanoparticles[22]. However, no fibrillar assembly of nanoparticles was observed in the absence of fatty acid salts (Supplementary Fig. 1). As explained below, we evaluate the capillary interaction energy between the nanoparticles to be at least an order of magnitude higher than the magnetic residual dipolar attraction energy (Supplementary Fig. 3).

Multi scale characterization of the structure of the dried magnetic chain-like assemblies was performed using scanning electron microscopy (SEM), transmission electron microscopy (TEM; see Supplementary Fig. 5) and atomic force microscopy (AFM, Fig. 2a). The filamentous assembly is 50–100 times thicker than a single chain of particles and probably results from magnetophoretic attraction of the nanoparticles to the high-intensity field region at the ends of the filaments, similar to the dielectrophoretic assembly of gold-nanoparticle microwires reported earlier[4]. AFM shows a thick fibre-like body of homogeneously distributed aggregated magnetic nanoparticles. The composition of the self-assembled fibrous structures was determined by thermogravimetric analysis (TGA). The weight loss curves for lauric acid with magnetic nanoparticles, plotted in Fig. 2b, show similar decomposition profiles for nanoparticle–fatty acid complexes in both the dispersed and field-aggregated state. The volume fraction of fatty acid in the filament assemblies is 0.4–0.5,

indicating that the constituent particles are embedded in a relatively thick shell of lipid. The first molecular layer of fatty acids is probably anchored on the iron oxide surfaces, as the terminal –COOH groups of lipids are known to have coordinating and chelating affinity to iron oxide[23]. This molecular layer completely wets the nanoparticle surfaces and modifies their physiochemical properties. The wetted surface further promotes condensation of lipid from its bulk dispersed forms, as visualized by cryo-TEM (Fig. 2c). The nanoparticles act as nuclei for the condensation of the lipid, resulting in the formation of thick shells around the particles. When the magnetic field pulls the nanoparticles and their clusters covered with lipid shells into contact, the capillary adhesion between these fluid shells binds the assembled nanoparticle fibre together.

The results indicate that the binding and formation of permanently assembled structures by nanocapillary forces depend critically on the presence of lipid shells in the fluid state around the particles. We proved this by a few complementary experimental studies. We characterized the state of C_{10}–C_{20} saturated fatty acid salts in the presence of Fe_2O_3 nanoparticles and correlated it to capillary binding. All fatty acid salts with the choline hydroxide counterion had a phase transition below 10 °C (Supplementary Fig. 7) and filament assembly was observed for all tested homologous lipids. For fatty acid ethanolamine salts, the phase-transition temperature as determined by differential scanning calorimetry (DSC), increases with the number of carbon atoms of the acid. At 25 °C, for fatty acids above 14 carbon atoms, the shell was in a solidified (liquid crystalline or glassy) state (Fig. 2d). In excellent correspondence, the formation of permanent filaments with ethanolamine salts at 25 °C was observed only for fatty acids up to 14 C-atoms (open circles, Fig. 2d and Supplementary Table 1). Longer backbone fatty acids (>14 carbon atoms) with shells in the solidified phase did not show permanent assembly at 25 °C; however, when the temperature was increased above their corresponding phase transition—that is, when the lipid shell was melted to the sticky fluid state—permanently assembled fibres were obtained for all systems (open circles, Fig. 2d). Similarly, permanent filaments at 25 °C were assembled with the 18-carbon backbone oleic acid (monounsaturated) acid and 12-hydroxystearic acid, where the molecule kink produced by a double bond or side hydroxyl group leads to a decrease of the phase-transition temperature[24]. No assembly was observed for corresponding 18-carbon saturated stearic acid, which is in a solidified state (Supplementary Fig. 7).

The critical role of the lipid fluidity was further proved by two other means. First, we showed that the liquid bridges break on cooling through the phase transition. Indeed, the filaments assembled while the lipid was in the fluid state (for C-16 >40 °C) disintegrated when the system was cooled to temperatures below the lipid phase-transition point (Fig. 3a–c and Supplementary Movie 2). Second, the role of fluidity of the lipid shell on interparticle interaction was investigated by dynamic light scattering (DLS). The diffusion rate for particles with a solidified lipid shell state was constant, suggesting the absence of aggregation (Supplementary Fig. 8). In contrast, for nanoparticles with a lipid shell in the fluid state the autocorrelation function shifted to lower diffusion rates (that is, longer lag times), indicating self-aggregation on contact, as Brownian collisions between nanoparticles trigger the formation of fluid lipid capillary bridges. Overall, the DLS data confirm by another means that aggregation occurs only when the lipid shells surrounding the

nanoparticles are in the fluid state. Such particles remain into the micro-aggregated state even before applying the external magnetic field (Fig. 1c).

The nanoparticles are trapped in a short-range attractive potential well resulting from the capillary bridge formation. On the basis of the cryo-TEM images we estimated the typical nanocapillary force acting between the nanoparticles to be ∼0.5 nN (see Supplementary Information). These nanocapillary forces are comparable in magnitude to the forces responsible for the formation of clusters in freely falling granular matter[25]. Our calculations show that the capillary interactions would dominate the magnetic attraction at interparticle distances >1.2 nm (Supplementary Fig. 3). However, the osmotic pressure developed by the first molecularly anchored lipid layer restricts the interparticle separation to >2 nm, which prevents the irreversible magnetic binding and/or coagulation of nanoparticles into van der Waals attractive global minima. This steric repulsion is a prerequisite for maintaining the flexibility of the interparticle junctions. We predict that the particle-to-particle rollover torque in the nanocapillary bridges is nearly absent because of the low hysteresis of the receding and advancing contact angles over the particles completely wetted by condensed lipid[26]. This leads to the remarkably high flexibility of the nanoparticle filaments, which was evaluated as explained below.

The flexibility of chain-like and fibrillar objects after prolonged thermal equilibration can be correlated to the persistence length, which is the distance along the contour at which the filament 'forgets' its original orientation. It was determined by the decay in the tangent vector correlation function ($\langle\cos(\theta)\rangle$) along the filament contour (Fig. 3d inset) and is given by $\langle\cos\theta(x)\rangle = \exp(-x/l_p)$, where l_p is the persistence length and θ is the angle between tangents at any two points on the filament contour with distance x apart (for details see Supplementary Information). In the presence of an external magnetic field, the persistence length of the filaments exceeds their contour length, which further increases on increasing the applied magnetic field (data not shown). However, in the absence of the field, the persistence length for our filaments was estimated to be 26 μm (±10 μm), which corresponds to a flexural rigidity of $\simeq 1 \times 10^{-25}$ Nm^2. A size-independent unified representation of the flexibility of the chain-like structure on any length scale can be achieved by plotting the persistence length against the linear density (mass per unit length, λ_p). This universal dependence[27,28] of l_p on λ_p for a few synthetic and biological polymers, as well as various chain-like objects, is plotted in Fig. 3d. The persistence length is a quadratic function of linear mass density ($l_p = K\lambda_p^2$ where K is a constant, Fig. 3d, solid line)[27,28], and materials deviating from this quadratic dependence are considered as either ultra-rigid $(l_p \gg K\lambda_p^2)$ or ultrasoft $(l_p \ll K\lambda_p^2)$. One type of flexible chain reported earlier, also plotted in Fig. 3d, is DNA-linked magnetic beads[8]. Strikingly, the present nanoparticle filaments linked via capillary bridges are orders of magnitude more flexible than other known molecular and supramolecular linear structures (Fig. 3d). It should be emphasized that this apparent high flexibility is not a typical result of low mechanical tension, rather than emerging from fluid-mediated particle re-adjustment; thus, it presents an interesting topic for future theoretical interpretation.

The high flexibility of the filaments facilitated their unusual dynamics, leading to bending and self-closing in alternating magnetic field. The two most common closed structures resulting from timed switching of field direction were rings and infinity-shaped loops. The mechanistic pathways for the formation of these self-closed structures in a 2D plane are illustrated in Fig. 4a–e. The fibres in constant field were in a fully stretched linear configuration (Fig. 4a and Supplementary Movie 3). On reversing the direction of the applied field, they could follow the change in field polarization[29] by two intermediate curling pathways: cis-curling (Fig. 4b) and trans-curling (Fig. 4c). When the free ends of a filament in the dynamically morphing intermediates meet each other or the centre on the filament, they snap, forming a self-closed structure. These closed loop configurations are retained after switching off the external field.

The capillary interaction also leads to nanoparticle stickiness and a re-configurability that can be used to assemble more complex hierarchical structures by field-guided dynamics (Supplementary Movie 4). An unusual feature of the magnetically responsive filaments results from the fluidity of the capillary bridges, which can be broken and re-formed on demand. The reversibility of the capillary snapping suggests that severed filaments can reconnect and self-repair with application of the field. We demonstrate in Fig. 4f–h rudimentary examples of repairing a broken 2D percolated filament network by application of a magnetic field. First, the percolated network of filaments was locally damaged mechanically by a sharp stylus. The disconnected ends of the cut filaments were then readily repaired using an external magnetic field, as the ends attract each other in the field and readily snap back into contact, recovering the network (Fig. 4f–h and Supplementary Movie 5). As expected, the rate of filament reconnection is dependent on the regenerating magnetic field strength (not shown). The regenerative ability of this nanoparticle network is broadly analogous to molecularly self-repairing polymer materials[30].

In summary, we have demonstrated that attractive capillary bridging forces could be operational at the nanoscale and, in conjunction with an external magnetic field, provide a facile tool for assembling extremely flexible nanoparticle filaments and networks. The binding by soft-sticky capillary bridges has a number of unique features—reversible snapping on contact, easy rollover, and high sensitivity to temperature near the liquid–solid phase transition of the bridges. This multiphase liquid-mediated assembly of particles offers a tool for developing active and smart materials, such as hierarchical structures that can be dynamically reconfigured and actuated, thermo-responsive self-healing colloidal gels with potentially unusual magnetic and rheological responses, ultraflexible magneto-actuators for soft robotics, and artificial flagella for microrobotics.

Methods

Sample preparation

The nanocapillary binding of maghemite particles was accomplished with numerous fatty acids obtained from Sigma-Aldrich (purity > 90%). Fatty acid soaps were prepared by adding either ethanolamine (Sigma-Aldrich, 99% purity) or choline hydroxide (Sigma-Aldrich, 46 wt.% in H_2O) as counterion. The γ-Fe_2O_3 nanoparticle powder (mkNANO,

purity > 99%) was added to the fatty acid soap solution. The mixture was equilibrated at 80 °C and sonicated for 20 min before experiments.

DSC, TGA and DLS measurements

The lipid–nanoparticle dispersion was allowed to stand for 24 h before the supernatant with excess lipid was decanted. The lipid–nanoparticle slurry was dried at 40 °C for two days and further used for DSC and TGA experiments. DSC was performed using a TA Instruments DSC Q100 device with a dry nitrogen gas flow of 50 ml min^{-1}. Heating and cooling ramps were repeated twice from 10 to 80 °C at a ramping rate of 1 °C min^{-1}. TGA measurements were performed using a TA Instruments SDT Q600 thermal analysis system under an inert nitrogen atmosphere from 30 to 700 °C at a ramping rate of 5 °C min^{-1}. DLS measurements were performed on filtered aqueous lipid–nanoparticle dispersions using a Zetasizer Nano ZS (backscattering 173°, Malvern Instruments).

Microscopy

Optical—The microfilaments and their assemblies were monitored with an Olympus BX-61 microscope in bright-field mode. The temperature of the dispersion was precisely controlled by using a temperature controller microscope stage (PE 94 (Linkam Scientific Instruments)).

TEM—A drop of the sample was placed on a carbon-coated copper grid (Quantifoil) and air-dried. The sample was negatively stained with uranyl acetate (2% w/w) and observed using a JEOL JEM-1230 TEM operating at 80 kV.Cryo-TEM measurements were performed on the same instrument. Samples were prepared by common flash-freezing procedures and images were recorded under low-dose conditions.

AFM—The nanoparticle filaments were air-dried on a silicon substrate and the scanning was performed with pyramidal silicon nitride cantilevers (Micro Cantilever) in tapping mode. The images were recorded using a 5500 AFM (Agilent Technologies) at the lowest possible stable scanning force (15 nN).

Supplementary Material

Refer to Web version on PubMed Central for supplementary material.

Acknowledgments

The authors gratefully acknowledge support from the US National Science Foundation (NSF) Triangle MRSEC on Programmable Soft Matter (DMR-1121107) and the US Army Research Office (ARO) (W911NF-15-1-0115). M.R. acknowledges financial support from the NSF under grants DMR-1122483, DMR-1309892 and DMR-1436201, from the National Institutes of Health (NIH) under grants P01-HL108808 and 1UH2HL123645, and from the Cystic Fibrosis Foundation. A.L.F. thanks BIA-INRA Nantes for her new faculty fellowship. We gratefully acknowledge C. Gaillard for the cryo-TEM experiments done at the BIBS Plate-forme INRA Nantes, France. We acknowledge the experimental assistance of B. Houinsou-Houssou, N. Galinsky, J. Zhao and J. C. Ledford. We are also grateful to L. Reynolds, J. Tracy and G. H. Findenegg for discussions on the data and their interpretation.

References

1. Nie Z, Petukhova A, Kumacheva E. Properties and emerging applications of self-assembled structures made from inorganic nanoparticles. Nature Nanotech. 2010; 5:15–25.
2. Velev OD, Gupta S. Materials fabricated by micro- and nanoparticle assembly—the challenging path from science to engineering. Adv Mater. 2009; 21:1897–1905.
3. Grzelczak M, Vermant J, Furst EM, Liz-Marzan LM. Directed self-sssembly of nanoparticles. ACS Nano. 2010; 4:3591–3605. [PubMed: 20568710]
4. Hermanson KD, Lumsdon SO, Williams JP, Kaler EW, Velev OD. Dielectrophoretic assembly of electrically functional microwires from nanoparticle suspensions. Science. 2001; 294:1082–1086. [PubMed: 11691987]
5. Bharti B, Findenegg GH, Velev OD. Co-assembly of oppositely charged particles into linear clusters and chains of controllable length. Sci Rep. 2012; 2:1004. [PubMed: 23256038]
6. Hill LJ, Pyun J. Colloidal polymers via dipolar assembly of magnetic nanoparticle monomers. ACS Appl Mater Interfaces. 2014; 6:6022–6032. [PubMed: 24467583]
7. Singh H, Laibinis PE, Hatton TA. Synthesis of flexible magnetic nanowires of permanently linked core-shell magnetic beads tethered to a glass surface patterned by microcontact printing. Nano Lett. 2005; 5:2149–2154. [PubMed: 16277443]
8. Li D, Banon S, Biswal SL. Bending dynamics of DNA-linked colloidal particle chains. Soft Matter. 2010; 6:4197–4204.
9. Cohen-Tannoudji L, et al. Polymer bridging probed by magnetic colloids. Phys Rev Lett. 2005; 94:038301. [PubMed: 15698329]
10. Devries, Ga, et al. Divalent metal nanoparticles. Science. 2007; 315:358–361. [PubMed: 17234943]
11. Leunissen ME, et al. Switchable self-protected attractions in DNA-functionalized colloids. Nature Mater. 2009; 8:590–595. [PubMed: 19525950]
12. Hornbaker DJ, Albert R, Albert I, Barabasi AL, Schiffer P. What keeps sandcastles standing? Nature. 1997; 387:765.
13. Butt HJ, Kappl M. Normal capillary forces. Adv Colloid Interface Sci. 2009; 146:48–60. [PubMed: 19022419]
14. Min Y, Akbulut M, Kristiansen K, Golan Y, Israelachvili J. The role of interparticle and external forces in nanoparticle assembly. Nature Mater. 2008; 7:527–538. [PubMed: 18574482]
15. Koos E, Willenbacher N. Capillary forces in suspension rheology. Science. 2011; 331:897–900. [PubMed: 21330542]
16. Bowden N, Choi IS, Grzybowski BA, Whitesides GM, Street O. Mesoscale self-assembly of hexagonal plates using lateral capillary forces: Synthesis using the ‘capillary bond’. J Am Chem Soc. 1999; 121:5373–5391.
17. De Volder M, Hart AJ. Engineering hierarchical nanostructures by elastocapillary self-assembly. Angew Chem Int Ed. 2013; 52:2412–2425.
18. Doyle PS, Bibette J, Bancaud A, Viovy JL. Self-assembled magnetic matrices for DNA separation chips. Science. 2002; 295:2237. [PubMed: 11910102]
19. Cho EC, Shim J, Lee KE, Kim JW, Han SS. Flexible magnetic microtubules structured by lipids and magnetic nanoparticles. ACS Appl Mater Interfaces. 2009; 1:1159–1162. [PubMed: 20355906]
20. Bannwarth MB, et al. Well-defined nanofibers with tunable morphology from spherical colloidal building blocks. Angew Chem Int Ed. 2013; 52:10107–10111.
21. Klinkova A, Thérien-Aubin H, Choueiri RM, Rubinstein M, Kumacheva E. Colloidal analogs of molecular chain stoppers. Proc Natl Acad Sci USA. 2013; 110:18775–18779. [PubMed: 24190993]
22. Muxworthy AR, Williams W. Critical superparamagnetic/single-domain grain sizes in interacting magnetite particles: Implications for magnetosome crystals. J R Soc Interface. 2009; 6:1207–1212. [PubMed: 19091684]

23. Pichon BP, et al. 2D assembling of magnetic iron oxide nanoparticles promoted by SAMs used as well-addressed surfaces. J Phys Chem C. 2010; 114:9041–9048.
24. Rawicz W, Olbrich KC, McIntosh T, Needham D, Evans E. Effect of chain length and unsaturation on elasticity of lipid bilayers. Biophys J. 2000; 79:328–339. [PubMed: 10866959]
25. Royer JR, et al. High-speed tracking of rupture and clustering in freely falling granular streams. Nature. 2009; 459:1110–1113. [PubMed: 19553995]
26. Bico J, Ashmore-Chakrabarty J, McKinley GH, Stone HA. Rolling stones: The motion of a sphere down an inclined plane coated with a thin liquid film. Phys Fluids. 2009; 21:082103.
27. Rubinstein, M.; Colby, RH. Polymer Physics. Oxford Univ. Press; 2003.
28. Boal, D. Mechanics of the Cell. Cambridge Univ. Press; 2002.
29. Biswal SL, Gast AP. Rotational dynamics of semiflexible paramagnetic particle chains. Phys Rev E. 2004; 69:041406.
30. Ghosh B, Urban MW. Self-repairing oxetane-substituted chitosan polyurethane networks. Science. 2009; 323:1458–1460. [PubMed: 19286550]

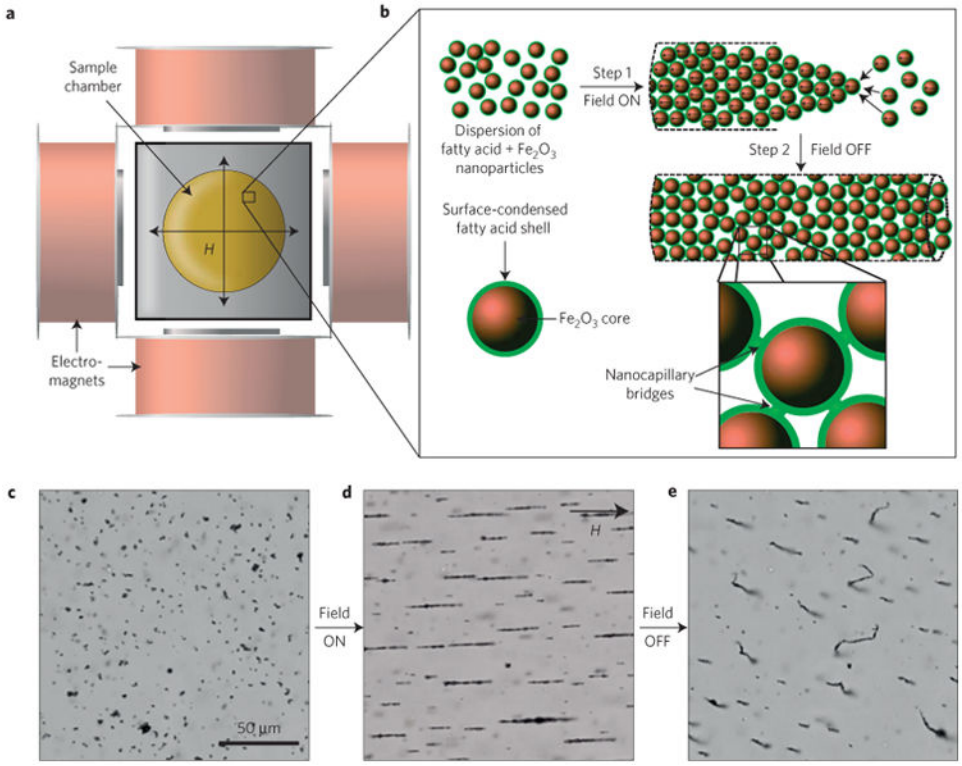

Figure 1. Magnetic assembly of permanent flexible nanoparticle filaments by nanocapillarity

a, Schematic of the experimental set-up. The sample chamber is surrounded by four electromagnets, producing uniform magnetic fields (*H*) of up to 15,000 Am^{-1}. **b**, Scheme of the filament-formation process (see also Supplementary Movie 1). Step 1: External magnetic-field-directed nanoparticle attraction and collection. Step 2: Permanent filaments persist after the field is switched off. **c**, Microscope image of magnetic particles and lipid dispersion before applying the field. **d**, Linear filaments formed by the particles in the direction of an applied field of 1,200 Am^{-1} after 1 min. **e**, Flexible filamentous structures undulating freely in the absence of an applied magnetic field.

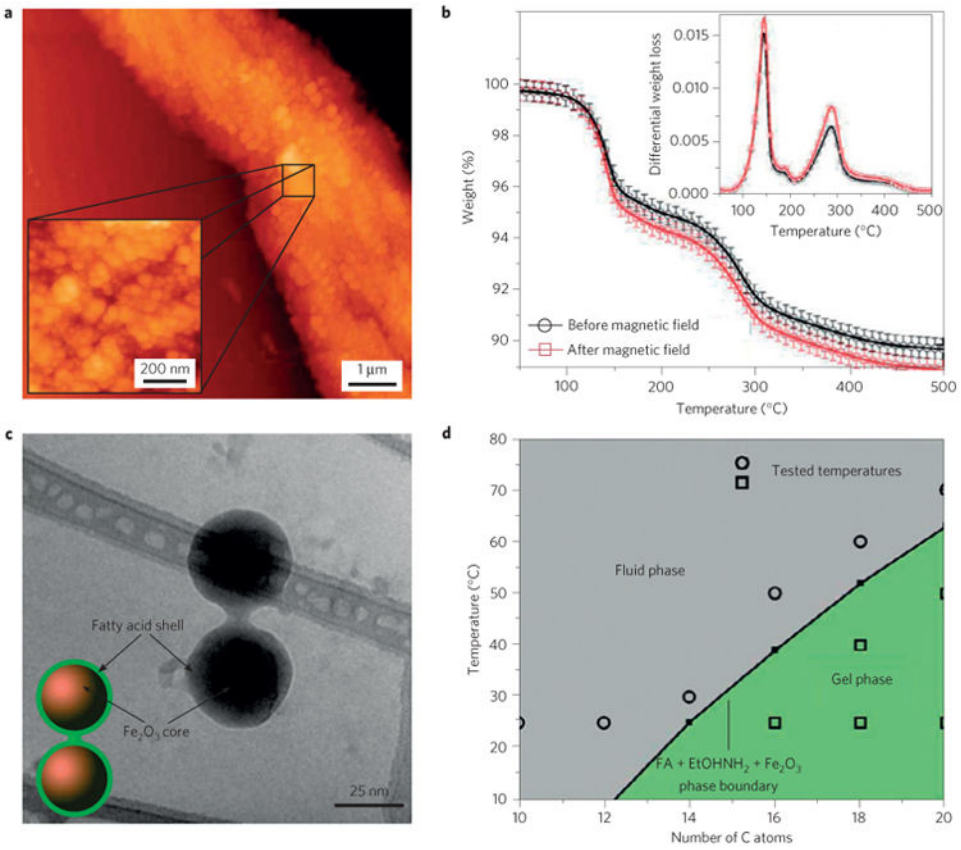

Figure 2. The composition of the filaments reveals the role of the lipid in nanoparticle assembly

a, AFM image of a lipid-Fe_2O_3 filamentous structure in the dried state. **b**, Thermogravimetric weight loss and corresponding differential weight loss (inset) profiles for Fe_2O_3 nanoparticles with lauric acid in the dispersed (open circles) and the assembled state (open squares). **c**, Cryo-TEM micrograph showing the presence of a thick lipid shell on the nanoparticle surface and the formation of a bridge between two nanoparticles. **d**, Phase-transition temperatures of the shell between the gel and fluid phase for different number of C atoms in the lipids compared to filament formation. Filaments are observed only when the lipid is in the fluid state (open circles) and never when it is in a solid-like phase (open squares). The error bars in **b** correspond to the maximal possible error in the weight measurement during TGA experiments.

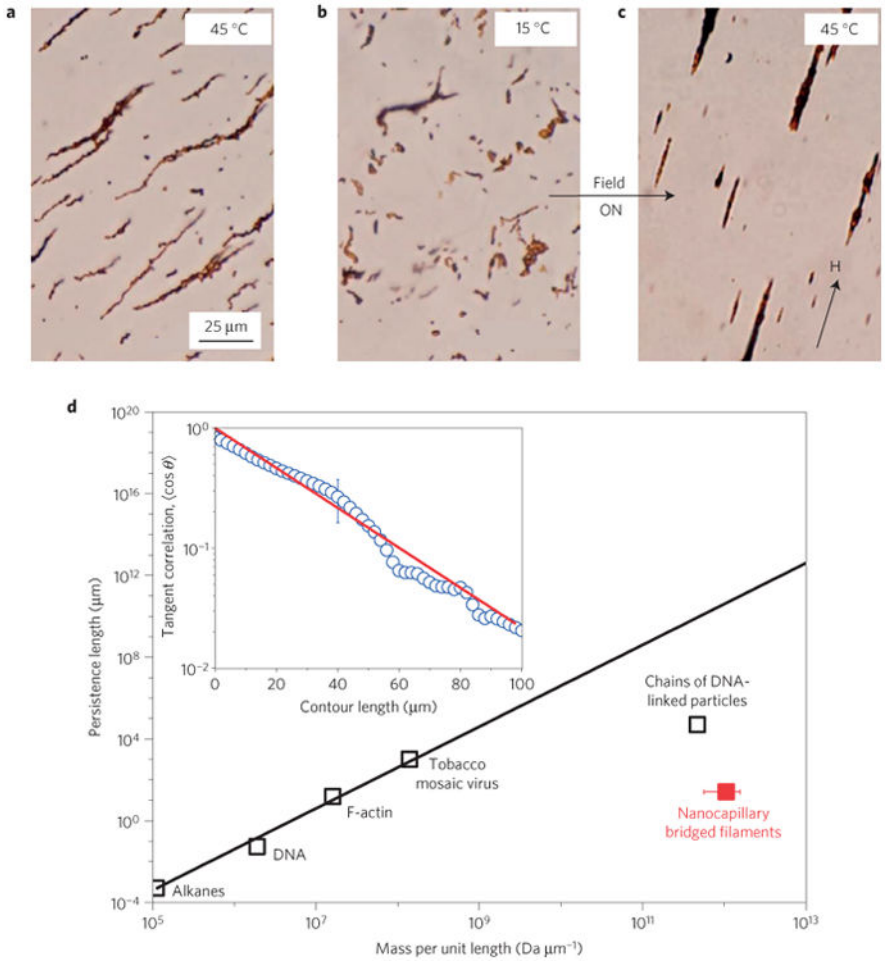

Figure 3. Experimental examples of phase-transition disintegration and characterization of the ultrahigh flexibility of the nanocapillary-bound filaments

a, Micrograph of the filaments assembled from a liquid C16-fatty acid salt at 45 °C (Supplementary Movie 2). **b**, These filaments break up on freezing the nanocapillary bridges between the particles. The fluid-to-gel-like transition in the present case is at 40 °C (Fig. 2d). **c**, The disintegrated filaments can be re-formed on increasing the temperature beyond the phase-transition temperature and applying an external magnetic field. **d**, Comparison of the intrinsic filament flexibility with that of macromolecules and linear biological assemblies. The persistence length of polymers and various linear objects is plotted as a function of their linear mass density. The persistence length of the filaments was determined by the decay of the tangent vector correlation function ($\langle \cos(\theta) \rangle$) along a filament contour (inset). The discrete points represent the experimental values and the line is the corresponding fit (for details see text). The error bars correspond to the standard deviation of the mean values of the tangential angle and mass per unit length. The standard deviation of the persistence length is less than the symbol size.

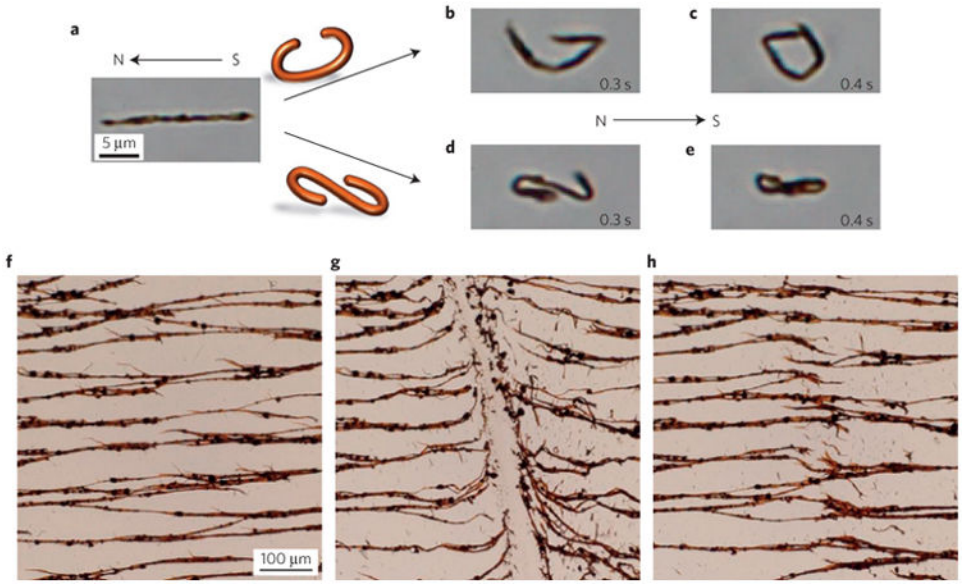

Figure 4. Examples of self-closing and magnetic repair of sticky filaments

a–e, Formation of self-closing structures in time-switched magnetic fields. **a**, A linear magnetic filament is aligned in the direction of the magnetic field. **b**,**d**, Cis- and trans-curling pathways followed by the filament on field reversal. **c**,**e**, Self-closed equilibrium ring and infinity-shaped structures attained by the flexible assemblies (see Supplementary Movie 3). **f**, Magneto-responsive 2D gel-like percolated network formed by the sticky filaments following an initial burst of magnetic field. **g**, Mechanically fractured network cut with a sharp stylus. **h**, After applying a magnetic field of intensity 1,200 Am^{-1}, the filaments are reconnected again owing to the stickiness, highlighting the self-repairing properties of this network (see also Supplementary Movie 5).